

## Order-by-disorder in the $XY$ pyrochlore antiferromagnet

Paul A. McClarty,<sup>1,2,3</sup> Pawel Stasiak,<sup>1,4</sup> and Michel J. P. Gingras<sup>1,5,6</sup>

<sup>1</sup>*Department of Physics and Astronomy, University of Waterloo, Waterloo, Ontario N2L 3G1, Canada*

<sup>2</sup>*Max Planck Institute for the Physics of Complex Systems, Nöthnitzer Straße 38, Dresden 01187, Germany*

<sup>3</sup>*ISIS Neutron and Muon Source, STFC, Rutherford Appleton Laboratory, Harwell Oxford, Didcot OX11 0QX, UK*

<sup>4</sup>*School of Mathematical and Physical Sciences, University of Reading, Whiteknights, Reading RG6 6AX, UK*

<sup>5</sup>*Canadian Institute for Advanced Research, 180 Dundas Street West, Suite 1400, Toronto, Ontario M5G 1Z8, Canada*

<sup>6</sup>*Perimeter Institute for Theoretical Physics, 31 Caroline Street North, Waterloo, Ontario N2L 2Y5, Canada*

(Received 18 August 2011; revised manuscript received 20 December 2013; published 31 January 2014)

We investigate the properties of the  $XY$  pyrochlore antiferromagnet with infinite local  $\langle 111 \rangle$  planar anisotropy. We identify the ground states and show that the configurational ground state entropy is subextensive. By computing the free energy due to harmonic fluctuations and by carrying out Monte Carlo simulations, we find that the model exhibits thermal order-by-disorder leading to low-temperature long-range order consisting of discrete magnetic domains. In doing so, we set aside doubts that order-by-disorder survives in the thermodynamic limit in this model. We compute the spin wave spectrum and show that thermal and quantum fluctuations select the same magnetic structure. With a previously unreported finite-size scaling analysis of Monte Carlo data, we confirm that the transition is first order for the  $XY$  model. Using Monte Carlo simulations, we find that the state selected by thermal fluctuations in this  $XY$  pyrochlore antiferromagnet can survive the addition of sufficiently weak nearest-neighbor pseudo-dipolar interactions or long-range dipolar interactions to the spin Hamiltonian. Quite interestingly, the resulting state selected by thermal order-by-disorder is metastable below some temperature. We discuss our results in relation to the  $\text{Er}_2\text{Ti}_2\text{O}_7$  and  $\text{Er}_2\text{Sn}_2\text{O}_7$  pyrochlore antiferromagnets.

DOI: [10.1103/PhysRevB.89.024425](https://doi.org/10.1103/PhysRevB.89.024425)

PACS number(s): 75.10.Dg, 75.10.Jm, 75.40.Cx, 75.40.Gb

### I. INTRODUCTION

The geometric frustration of magnetic interactions on lattices of magnetic moments often leads to a configurational classical ground state entropy that scales with the volume of the system,  $V$ , as  $V^\alpha$  with  $0 < \alpha \leq 1$ . This can have some unusual consequences. A well-known example is the Ising model on the triangular lattice with nearest-neighbor antiferromagnetic interactions which has an extensive ground state entropy ( $\alpha = 1$ ) and exhibits no finite-temperature transition [1]. While in real materials a  $V^\alpha$  entropy left by the leading interactions is often energetically lifted by weaker interactions, leading to long-range magnetic order, there are some exceptions. For example, in the  $\text{Dy}_2\text{Ti}_2\text{O}_7$  and  $\text{Ho}_2\text{Ti}_2\text{O}_7$  spin ice materials [2], in which the magnetic moments are described by Ising spins, the extensive ( $\alpha = 1$ ) low-temperature entropy caused by frustration of the leading effective ferromagnetic nearest-neighbor interactions is indeed lifted by the perturbing long-ranged part of the dipolar interaction [3–5]. However, the degeneracy lifting in this system is so weak that the theoretically expected phase transition to magnetic long-range order, in most experiments, is inhibited by a freezing into a spin ice state without long-range order [6,7]. See, however, Ref. [8].

Another possibility for a system with an exponentially ( $\exp[CV^\alpha]$ ) large number of classical degenerate ground states is that thermal or quantum fluctuations might select a subset of states about which the density of zero modes is greatest. These entropic and quantum state selection mechanisms are both referred to as order-by-disorder (OBD) [9–12]. Among pyrochlore antiferromagnets, in which the spins sit on a lattice of corner-sharing tetrahedra, Moessner and Chalker have given a criterion for the occurrence of long-range order induced by thermal fluctuations [13]. This criterion is based on the

degree of divergence of the statistical weight of particular spin configurations—a power-counting argument depending on the number of zero-energy excitations (zero modes) for a given spin configuration and the number of dimensions of the ground state manifold. For example, this criterion indicates that the  $XY$  antiferromagnet with globally coplanar spins (spins perpendicular to the global  $[001]$  axis) should exhibit entropic selection—a result which is borne out by Monte Carlo simulations [13]. For such  $XY$  systems, this comes about because the number of zero modes about collinear spin configurations is proportional to the number of spins whereas the configurational entropy in the ground state is subextensive, growing as  $V^{2/3}$  [13,14].

This article is concerned with the pyrochlore  $XY$  antiferromagnetic model with local  $\langle 111 \rangle$  spins, meaning that there is a different easy plane for each of the four tetrahedral sublattices [14–17]. Because such a model preserves the cubic symmetry of the pyrochlore lattice and because the single-ion crystal field can, and does in various materials [18], generate such an anisotropy, it is more physical than the aforementioned pyrochlore  $XY$  model with a global easy plane [13]. The model was recognized some time ago to exhibit a continuous degeneracy in its classical ground state [16,17]. Monte Carlo simulations of the local  $\langle 111 \rangle$   $XY$  antiferromagnet [14,16,17] indicate that it exhibits two phases—a high-temperature paramagnetic phase and a low-temperature long-range-ordered phase. We refer to the magnetic structure in the ordered phase as  $\psi_2$  (which is one component of the  $\Gamma_5$  branch of degeneracies in the classical  $XY$  antiferromagnet) to be consistent with Ref. [19] and the group theory literature. A calculation of the spectrum of the Hessian about different discrete ground states [16] suggests that the observed long-range-ordered spin configuration in Monte Carlo simulations has the largest density of zero modes of all the degenerate ground states and,

consequently, that the transition observed in the simulations is an example of classical (thermal) OBD [16,17]. However, the authors of Ref. [16] did question whether the selection of the long-range-ordered  $\psi_2$  state survives in the thermodynamic limit.

In this article, we expand on the work of Refs. [16,17] and give a more systematic account of the properties of the local  $\langle 111 \rangle$  XY pyrochlore. We present in Sec. II the model and its ground states. In Sec. III, we discuss some of the details of the Monte Carlo simulations performed in this work. Section IV reports results of an analytical and numerical investigation of the thermal order-by-disorder mechanism, providing definitive evidence that the fluctuation selection mechanism of the  $\psi_2$  state does survive in the thermodynamic limit and giving further insight into the mechanism leading to order-by-disorder than was previously given [16,17]. We also include in Sec. IV a subsection showing that there is a quantum order-by-disorder mechanism in the XY model as speculated but not shown in Ref. [15]. More recent work [20] building on the preprint version of the present work [21] has confirmed this result.

In Sec. V we put the model considered in this paper in the context of the phenomenology of the rare-earth pyrochlores and, in particular, the material  $\text{Er}_2\text{Ti}_2\text{O}_7$ . Specifically, we discuss how the XY model controls the physics over a significant part of the space of couplings of pyrochlore magnets. We also consider the problem of the stability of the long-range order selected by thermal order-by-disorder when there is a weak competition with an energetically selected magnetic order. In particular, we discuss the effect of weak dipolar interactions on the XY antiferromagnet of either nearest-neighbor of exchange origin or true long-range  $1/r^3$  nature and of magnetostatic origin. We conclude the paper with a brief discussion in Sec. VI.

## II. MODEL

In this work, we mostly focus on the problem of the zero and finite-temperature behavior of interacting classical spins of fixed length on the sites of a pyrochlore lattice of corner-sharing tetrahedra with an infinite single-ion anisotropy such that the spins lie within their respective local XY planes perpendicular to the local  $\langle 111 \rangle$  directions. In Sec. IV B, we discuss the problem of order-by-disorder due to quantum fluctuations in a model with spin operators  $\mathbf{S}$  [14–16].

The interactions are taken to be antiferromagnetic isotropic exchange between nearest neighbors with coupling  $J$  ( $J > 0$ ). Later on we also consider, as a perturbation, both pseudo-dipolar interactions solely between nearest neighbors with coupling strength  $\mathcal{D}$  and long-range dipolar interactions with the same coupling. First we introduce a Hamiltonian in terms of angular momentum  $\mathbf{J}$ :

$$H = J \sum_{(i,j)} \mathbf{J}_i \cdot \mathbf{J}_j + \mathcal{D} R_{\text{nn}}^3 \sum_{\text{pairs}} \left( \frac{\mathbf{J}_i \cdot \mathbf{J}_j}{|\mathbf{R}_{ij}|^3} - \frac{3(\mathbf{J}_i \cdot \mathbf{R}_{ij})(\mathbf{J}_j \cdot \mathbf{R}_{ij})}{|\mathbf{R}_{ij}|^5} \right), \quad (1)$$

where  $R_{\text{nn}}^3$  is the nearest-neighbor distance. For the case of pseudo-dipolar interactions, the dipolar interaction in the above formula is truncated beyond nearest neighbors. We

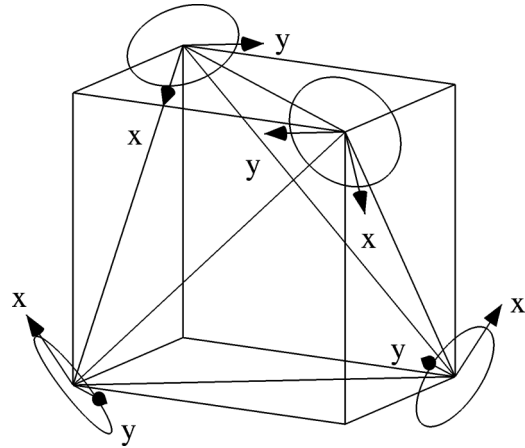


FIG. 1. The local XY easy planes and the local coordinates for each of the tetrahedral sublattices shown on the vertices of a single tetrahedron. The local spin angles,  $\phi_a$  (for sublattices  $a = 1, 2, 3, 4$ ), are measured from the  $x$  axes. The local  $z$  axes (not shown) point in the local  $\langle 111 \rangle$  directions towards the center of the tetrahedron.

consider both the nearest-neighbor part of the dipole and the long-range magnetostatic dipole for the sake of completeness. The dipolar interaction may arise between nearest neighbors as one component of the four symmetry-allowed exchange couplings on the pyrochlore lattice [22–24] while the long-range dipolar interaction is simply a magnetostatic coupling between the elementary dipole moments. However, the classical ground states of both the full long-range dipolar interaction model and those of the nearest-neighbor dipolar interaction model are the same [25]. We would expect that the long-range part of the dipolar interaction should not change the qualitative physics introduced by the nearest-neighbor dipolar coupling because the tetrahedra for the ordered magnetic structures considered here have zero moment. Our simulation results in Sec. V confirm this naive expectation.

In the following we adopt a set of coordinate axes particular to each of the four pyrochlore sublattices. The convention that we choose is illustrated in Fig. 1. In order to impose the single-ion anisotropy on the moments, we rotate each angular momentum  $\mathbf{J}$  into the local  $\langle 111 \rangle$  coordinate system on every site and we make the transformation

$$(\mathbf{J}^x, \mathbf{J}^y, \mathbf{J}^z) \rightarrow (g_{\perp} S^x, g_{\perp} S^y, g_{\parallel} S^z), \quad (2)$$

where the  $g$  factor components,  $(g_{\perp}, g_{\perp}, g_{\parallel})$ , may vary continuously between Ising-like moments with  $g_{\perp} = 0$  to local XY moments with  $g_{\parallel} = 0$ . One way of viewing this transformation is as a projection of the bare superexchange couplings between moments  $\mathbf{J}$  in Eq. (1) onto the crystal field doublet ground states on each magnetic site rendered in terms of pseudospins  $\mathbf{S} = 1/2$  [24,26].

Consider first the exchange-only model with  $\mathcal{D} = 0$ . In this case, the Hamiltonian in Eq. (1) can be put into the form  $H_{\text{ex}} = (J/2) \sum_{\text{t}} (\mathbf{S}_{\text{t}}^2 - 4S^2)$ , where the sum runs over all connected tetrahedra [13] and  $\mathbf{S}_{\text{t}}$  is the total spin on each tetrahedron. It follows that the ground states are all those states with zero net “spin” ( $\mathbf{S}_{\text{t}} = 0$ ) on each tetrahedron. Therefore, we write down the conditions for the three components of the total spin on a tetrahedron to be zero. In doing so, we impose the XY

constraint so that the orientation of spin  $a$  (for sublattices  $a = 1, 2, 3, 4$ ), is given by a single angle  $\phi_a$  measured with respect to axes within the local plane (normal to the relevant local [111] direction) shown in Fig. 1 and given in Ref. [23]. The condition of zero net spin on each tetrahedron can then be written as

$$\begin{aligned}\cos(\phi_1) + \cos(\phi_2) &= \cos(\phi_3) + \cos(\phi_4), \\ \cos(\phi'_1) + \cos(\phi'_4) &= \cos(\phi'_2) + \cos(\phi'_3), \\ \cos(\phi''_1) + \cos(\phi''_3) &= \cos(\phi''_2) + \cos(\phi''_4),\end{aligned}$$

where  $\phi'_a \equiv \phi_a + \frac{2\pi}{3}$  and  $\phi''_a \equiv \phi_a + \frac{4\pi}{3}$ . There are four solution branches to these equations [16]. Each branch corresponds to a continuous degeneracy wherein all four spins are rotated smoothly within their respective local [111] XY plane.

We place an overbar on  $\phi_a$  ( $\bar{\phi}_a$ ) to signify the angle for sublattice  $a$  giving an energy minimum (zero spin  $S_t$  on each tetrahedron). Then, we label the above branch solutions in the following way:

$$\begin{aligned}\text{branch 1: } \bar{\phi} &\equiv \bar{\phi}_1 = \bar{\phi}_2 = \bar{\phi}_3 = \bar{\phi}_4, \\ \text{branch 2: } \bar{\phi} &\equiv \bar{\phi}_1 = \bar{\phi}_2 = -\bar{\phi}_3 = -\bar{\phi}_4, \\ \text{branch 3: } \bar{\phi} &\equiv \bar{\phi}_1 = \bar{\phi}_3, \quad \frac{4\pi}{3} - \bar{\phi} = \bar{\phi}_2 = \bar{\phi}_4, \\ \text{branch 4: } \bar{\phi} &\equiv \bar{\phi}_1 = \bar{\phi}_4, \quad \frac{2\pi}{3} - \bar{\phi} = \bar{\phi}_2 = \bar{\phi}_3.\end{aligned}\tag{3}$$

A further discussion on how these solutions are rigorously found is given in Appendix A. We illustrate the spin configurations for two of the branches in Figs. 2 and 3.

To enumerate all the ground states on the pyrochlore lattice we first tile all the tetrahedra with a particular spin configuration from, say, branch 1. Then, we choose a line of

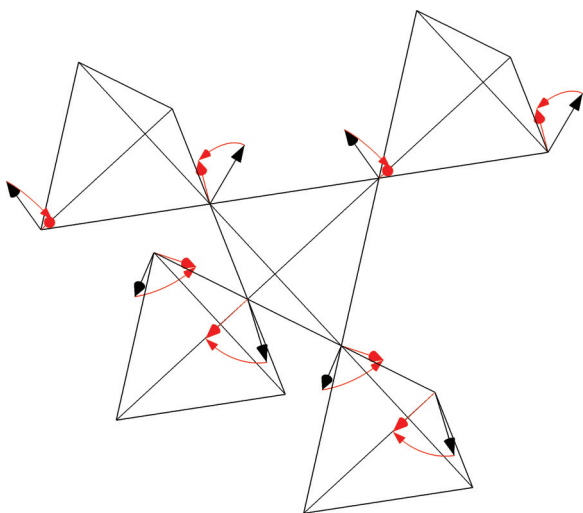


FIG. 2. (Color online) Collective spin rotation along a part of branch 1 of the continuous ground state, starting from  $\bar{\phi} = 0$  and progressing to  $\bar{\phi} = \pi/3$  [see Eq. (3)]. The red, arched arrows show the directions of rotation, starting from  $\bar{\phi}_a = 0$  (for sublattices  $a = 1, 2, 3, 4$ ), one of the  $\psi_2$  states, and ending in another  $\psi_2$  state, given by  $\bar{\phi}_a = \pi/3$ . The initial spin directions,  $\bar{\phi}_a = 0$ , are indicated with black arrows, and the final directions,  $\bar{\phi}_a = \pi/3$ , are shown with red arrows.

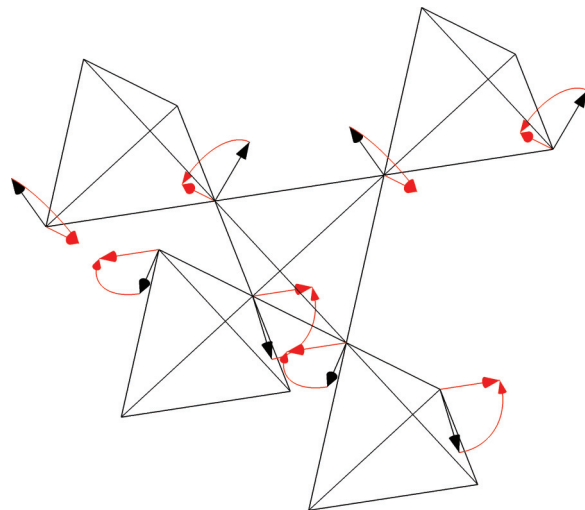


FIG. 3. (Color online) Collective spin rotation along a part branch 2 of the continuous ground state, starting from  $\bar{\phi} = 0$  and progressing to  $\bar{\phi} = \pi/2$  [see Eq. (3)]. The initial  $\bar{\phi}_a = 0$   $\psi_2$  state is shown with black arrows. The final configuration, indicated by red arrows, is the  $\psi_4$  state given by  $\bar{\phi}_1 = \bar{\phi}_2 = \pi/2$  and  $\bar{\phi}_3 = \bar{\phi}_4 = 3\pi/2$  [see Eq. (4)].

nearest-neighbor spins traversing the length  $L$  of the system. The sublattice labels of the spins on the so-defined chain alternate between two values  $a$  and  $b$ . There are six such pairs of labels. One can then transform the spins along the chain so that the spin configurations of the associated tetrahedra belong to another branch of solutions. For example, consider a single chain made of sublattices 3 and 4. All the local angles along this chain are identical initially and equal to, say,  $\theta$ . We can transform these to  $-\theta$  with no energy cost. Therefore, the entropy within the ground state manifold scales as  $L^2$  as first noted in Ref. [14]. This is in contrast to both the Heisenberg pyrochlore antiferromagnet and the global easy axis (Ising) pyrochlore antiferromagnet both of which have an extensive entropy.

We note that the four branches in Eq. (3) intersect in pairs. These intersection points are at special sublattice angles  $\bar{\phi} = n\pi/3$  with integer  $n$ . We refer to these as  $\psi_2$  states in the rest of this article [19]. By exploiting these intersection angles to move between the branches, one can smoothly visit all the ground states on a single tetrahedron and, indeed, on the whole pyrochlore lattice. If we return to the above chain of sublattices 3 and 4, the  $\bar{\phi} = 0$  configuration allows the tetrahedra along this chain to pass smoothly from branch 1 to branch 2. As shown in Refs. [15,16] and in Sec. IV below, thermal fluctuations have the effect of selecting a magnetic structure with  $\mathbf{q} = 0$  ordering wave vector and spin orientations at these discrete  $\bar{\phi}$  angles. There are six distinct  $\psi_2$  ground states which are the six  $\mathbf{q} = 0$  ordered states with tetrahedra tiled with local angles  $\bar{\phi}_a = n\pi/3$  for sublattices  $a = 1, 2, 3, 4$  and with integer  $n$ . One can take the observation that the lattice zero modes are along sublattice chains to understand an aspect of the Monte Carlo results of Ref. [16]—in particular, the finite-size scaling of the average energy of the  $\psi_2$  states at low temperature, which was not adequately determined in Ref. [16]. Since this point is somewhat removed from the main story of our paper, we present the argument in Appendix C.

For any  $\mathcal{D} \neq 0$ , a discrete set of ground states with  $\mathbf{q} = 0$  ordering wave vector is selected from the manifold of states described above. These energetically selected states are referred to as the  $\psi_4$  states [19,27] or Palmer-Chalker states in the literature after Ref. [25]. The angles specifying the  $\psi_4$  states are

$$\begin{aligned} \text{state 1: } \bar{\phi}_1 = \bar{\phi}_2 = \frac{\pi}{2}, \quad \bar{\phi}_3 = \bar{\phi}_4 = \frac{3\pi}{2}, \\ \text{state 2: } \bar{\phi}_1 = \bar{\phi}_3 = \frac{7\pi}{6}, \quad \bar{\phi}_2 = \bar{\phi}_4 = \frac{\pi}{6}, \\ \text{state 3: } \bar{\phi}_1 = \bar{\phi}_4 = \frac{11\pi}{6}, \quad \bar{\phi}_2 = \bar{\phi}_3 = \frac{5\pi}{6}, \end{aligned} \quad (4)$$

and the time-reversed configurations. In anticipation of what follows in Sec. V, we note that the  $\psi_4$  states are the ground states one finds for antiferromagnetic nearest-neighbor exchange with sufficiently weak nearest-neighbor pseudo-dipolar as well as for true  $1/r^3$  long-range magnetostatic dipolar interactions in the classical Heisenberg pyrochlore antiferromagnet model [25,28,29]. Interestingly, the  $\psi_4$  states are found experimentally to be the ground state of the  $\text{Gd}_2\text{Sn}_2\text{O}_7$  pyrochlore antiferromagnet [29–31], but not of the closely related  $\text{Gd}_2\text{Ti}_2\text{O}_7$  material [32,33].

### III. MONTE CARLO METHOD

In Secs. IVC and V below, we report results from Monte Carlo simulations of the local  $\langle 111 \rangle$  XY pyrochlore antiferromagnet. In this section, we give details of the Monte Carlo algorithm and the observables that were measured in the Monte Carlo simulations.

The Monte Carlo simulations were performed using parallel tempering [34] in which  $N_T$  replicas of a system of  $N$  spins, each at a different temperature and with a different series of pseudorandom numbers, are simulated simultaneously. In addition to local spin moves, parallel tempering swaps that exchange configurations between a pair of temperatures are attempted. The configuration swap attempts are accepted or rejected based on a Metropolis condition that preserves detailed balance. Parallel tempering has been shown, in systems known to equilibrate slowly using other methods, to improve performance substantially [34]. Replica swaps are attempted with a frequency of one attempt every 100 local Monte Carlo sweeps. A local Monte Carlo sweep consists of  $N$  spin move attempts. In our simulations,  $N_T = 64$  with either a constant increment between the temperatures, or with the temperatures self-consistently adjusted to obtain a uniform parallel tempering acceptance rate.

With each spin carrying a single angular coordinate  $\phi_i$ , the local spin moves involve choosing an angle increment  $\delta\phi_i$  from a uniform distribution between  $-\delta\phi_{\max}$  and  $\delta\phi_{\max}$ . The angle of spin  $\mathbf{S}_i$  was updated to  $\phi_i + \delta\phi_i$  and each tentative spin rotation was accepted or rejected based on a Metropolis test. The maximum increment  $\delta\phi_{\max}$  was updated every 100 Monte Carlo moves in order to maintain the spin move acceptance rate at 50%.

Physical observables were computed every 100 Monte Carlo sweeps. To determine the development of long-range order with ordering wave vector  $\mathbf{q} = 0$  (expected for sufficiently small  $\mathcal{D}/J$  in the model discussed above [25,28,29]),

the sublattice magnetization was computed [14]:

$$M_4 = \left\langle \sqrt{\frac{1}{4} \sum_{a=1}^4 \left( \frac{1}{N_P} \sum_{i=1}^{N_P} \mathbf{S}_{i,a} \right)^2} \right\rangle_{\text{th}}, \quad (5)$$

where each spin carries an fcc lattice label  $i$  and a sublattice label  $a$  (see Ref. [35]) and the number of sites in the lattice is  $N \equiv 4N_P$ , where  $N_P$  is the number of fcc (primitive lattice) sites. The angled brackets  $\langle \dots \rangle_{\text{th}}$  denote a thermal average. In order to distinguish the  $\psi_2$  (Refs. [15,19]) and  $\psi_4$  (Refs. [19,25]) phases, we introduce unit vectors  $\hat{\mathbf{e}}_a^{(\gamma(d))}$  which are oriented in the expected spin directions on each sublattice  $a$  for magnetic structure identified by the label  $\gamma$  with the domains labeled  $d$ , for both the  $\gamma = \psi_2$  and  $\gamma = \psi_4$  structures. From the combination

$$\Psi^{(\gamma(d))} = \frac{1}{N_P} \sum_{i=1}^{N_P} \sum_{a=1}^4 \mathbf{S}_{i,a} \cdot \hat{\mathbf{e}}_a^{(\gamma(d))}, \quad (6)$$

we compute the order parameter

$$q_\gamma = \left\langle \sum_d (\Psi^{(\gamma(d))})^2 \right\rangle_{\text{th}}, \quad (7)$$

for the  $\gamma = \psi_2$  (Refs. [15,19]) and  $\gamma = \psi_4$  (Refs. [19,25,27]) magnetic structures. In Eq. (7), the sum is taken over a choice of three out of the six magnetic domains, for each of these two structures, which are not related to one another by time reversal. The spin directions corresponding to the domains for  $\psi_4$  and  $\psi_2$  are given in Sec. II:  $\psi_4$  in Eq. (4) and for  $\psi_2$  all angles  $\bar{\phi}_a = n\pi/3$ . The order parameter for the  $\psi_4$  state  $q_{\psi_4}$  is the same one computed in the simulations of Ref. [36]. The magnetic specific heat per spin was computed from the fluctuations in the total energy of the system.

The sensitivity of the results to the initial spin configurations was assessed by comparing the results of simulations starting from (i) random configurations with a different configuration for each thermal replica, (ii)  $\psi_2$  ordered states, and (iii)  $\psi_4$  ordered states. We confirmed, in the case of the model without perturbing dipolar interactions [ $\mathcal{D} = 0$  in Eq. (1)], that equilibration was reached for each simulation, by checking that the results were independent of initial conditions. Also, the evolution of the order parameters was monitored during the course of each simulation to ensure that they reached a stationary state before the statistics were collected. Equilibration issues are discussed further in Sec. IVC and, for the case of the perturbed XY model, in Sec. V.

### IV. ORDER-BY-DISORDER

In this section, we consider the exchange-only model ( $\mathcal{D} = 0$ ) given in Eq. (1). General arguments given in Ref. [13] indicate that the XY antiferromagnet with globally coplanar spins should exhibit a thermally driven order-by-disorder transition. This argument does not straightforwardly carry over to the noncoplanar  $\langle 111 \rangle$  XY antiferromagnet. Simulation evidence for thermal order-by-disorder in the local  $\langle 111 \rangle$  XY model transition was presented in Refs. [14–17]. The classical degeneracies of this model were identified in Ref. [16] and order-by-disorder was found via Monte Carlo simulations.

However, the possibility had been mentioned in Ref. [16] that the temperature at which long-range order with a nonzero  $\psi_2$  order parameter develops might vanish in the thermodynamic limit. We present simulation results which provide compelling evidence that, for the exchange-only ( $D = 0$ ) model, a first-order phase transition to a long-range-ordered  $\psi_2$  state persists in the thermodynamic limit. We begin, however, with a previously unreported calculation of the free energy that considers harmonic fluctuations which clearly demonstrates a thermal  $\psi_2$  order-by-disorder in the thermodynamic limit without having to rely on Monte Carlo simulations. Then, having investigated the order-by-disorder mechanism in the exchange-only ( $D = 0$ ) model, we discuss in Sec. V the effect of competing nearest-neighbor pseudo-dipolar ( $D \neq 0$ ) interactions and also the full long-range magnetostatic dipolar interactions.

### A. Computation of the free energy

In this section, we show that certain discrete spin configurations from the manifold of  $\mathbf{q} = 0$  ground states minimize the free energy computed from harmonic fluctuations about the classical ground states. We assume that every tetrahedron on the lattice is tiled with the same spin configuration (i.e., that the ordering wave vector is  $\mathbf{q} = 0$ ). If we constrain the ordering to be  $\mathbf{q} = 0$ , the spin configuration is fixed by specifying four angles  $\phi_a$ , one for each sublattice. Let the angles in a ground state configuration be denoted  $\bar{\phi}_a$  for which the ground state energy is  $H(\bar{\phi}_a) = NE_g$ , where  $N$  is the number of spins. We then consider small fluctuations  $\delta\phi_i$  about these angles  $\phi_i = \bar{\phi}_i + \delta\phi_i$ . The terms linear in  $\delta\phi_i$  vanish, so the Hamiltonian  $H = NE_g + H_2 + \dots$ , where  $H_2$  is the part harmonic in the angular deformations.  $H_2$  is written in  $\mathbf{k}$  space as  $H_2 = \sum_{\mathbf{k}, a, b} \delta\phi_a(\mathbf{k}) A^{ab}(\mathbf{k}) \delta\phi_b(-\mathbf{k})$ . Here,  $\delta\phi_a(\mathbf{k}) = (1/\sqrt{N_P}) \sum_{\mathbf{R}_\mu} \exp[i\mathbf{k} \cdot (\mathbf{R}_\mu + \mathbf{r}_a)] \delta\phi_a(\mathbf{R}_\mu)$ , where  $\mathbf{R}_\mu$  are the fcc lattice points and  $\mathbf{r}_a$  are the vectors for the tetrahedral basis (see Ref. [35] for notation convention). This choice of convention for the lattice labeling ensures that the Hessian  $A^{ab}(\mathbf{k})$  is real. The eigenvalues  $\lambda_A(\mathbf{k})$  of  $A^{ab}(\mathbf{k})$  are nonnegative, reflecting the stability of the ground states. The spectrum of  $A^{ab}$  is computed in  $\mathbf{k}$  space as a function of the ground state for each branch.

One finds that for the special minimum energy configurations  $\bar{\phi}_a = n\pi/3$  for  $a = 1, 2, 3, 4$ , the four eigenvalues,  $\lambda_A(\mathbf{k})$ , ( $A = 1, 2, 3, 4$ ) of the  $A^{ab}(\mathbf{k})$  Hessian take the form

$$\begin{aligned} \bar{\phi}_a = 0, \pi, & \quad \lambda_A = 1 \pm \cos(\mathbf{k} \cdot \mathbf{r}_{12}), \quad 1 \pm \cos(\mathbf{k} \cdot \mathbf{r}_{34}), \\ \bar{\phi}_a = \pi/3, 4\pi/3, & \quad \lambda_A = 1 \pm \cos(\mathbf{k} \cdot \mathbf{r}_{13}), \quad 1 \pm \cos(\mathbf{k} \cdot \mathbf{r}_{24}), \\ \bar{\phi}_a = 2\pi/3, 5\pi/3, & \quad \lambda_A = 1 \pm \cos(\mathbf{k} \cdot \mathbf{r}_{23}), \quad 1 \pm \cos(\mathbf{k} \cdot \mathbf{r}_{14}), \end{aligned}$$

where each row gives the four eigenvalues for the indicated particular set of  $\bar{\phi}_a$  ( $a = 1, 2, 3, 4$ ) angles and which correspond to the aforementioned  $\psi_2$  states. The vector  $\mathbf{r}_{ab}$  joins nearest neighbors with sublattice labels  $a$  and  $b$ . The  $\psi_2$  states are distinguished from the other ground states in having a much higher density of zero modes—2 planes of zero modes in the first Brillouin zone [16,17]. The planes come about because, at these angles, one can smoothly introduce defects into the system along (which are usually referred to as  $\alpha$  and  $\beta$ ) chains in the crystal [18], as described in Sec. II. At angles away

from the  $\psi_2$  states, one can still introduce chain defects but not continuously.

We now compute the free energy for each  $\mathbf{q} = 0$  configuration after dropping all terms in the Hamiltonian beyond the harmonic terms. The free energy  $F[\bar{\phi}]$  at inverse temperature,  $\beta$ , is given at the harmonic level by

$$F[\bar{\phi}] \approx NE_g - \frac{1}{\beta} \ln \left[ \left( \prod_{a, \mathbf{k}} \int d[\delta\phi_a(\mathbf{k})] \exp(-\beta H_2) \right) \right] \quad (8)$$

and hence

$$F[\bar{\phi}] \approx NE_g - \frac{N}{2\beta} \ln \left( \frac{\pi}{\beta} \right) + \frac{1}{2\beta} \sum_{\mathbf{k}} \ln[A(\mathbf{k})]. \quad (9)$$

In the limit as  $N \rightarrow \infty$ , the third (last) term on the right-hand side of Eq. (9) is  $\frac{N}{4} \frac{1}{(2\pi)^3} I_2$  with  $I_2 = \sum_A \int d^3\mathbf{k} \ln[\lambda_A(\mathbf{k})]$  for the four ground state branches given in Sec. II (see Appendix B for a discussion of the various prefactors of  $I_2$ ). We evaluate the integral numerically using a Monte Carlo method with  $10^8$  points, noting that the singularities for the  $\psi_2$  spin configurations are integrable because the integrals take the form  $\int_0^{k_0} dk \ln k$  for some cutoff  $k_0$  [37]. The results are shown in Fig. 4. Evidently,  $I_2$ , and consequently the free energy  $F[\bar{\phi}]$ , is minimized for the  $\psi_2$  states at  $\bar{\phi}_a = n\pi/3$  where pairs of branches meet.

It is often the case that one can simulate the effect of order-by-disorder into a collinear state by introducing a term into the Hamiltonian of the form

$$H_{\text{OBD}} = -|\Gamma| \sum_{i,j} (\mathbf{S}_i \cdot \mathbf{S}_j)^2 \quad (10)$$

that selects the most collinear spin configurations among the classical ground states (see, for example, Refs. [10,11]). The usual argument for the selection of such states is that collinear spin configurations have, among all states, fluctuations that

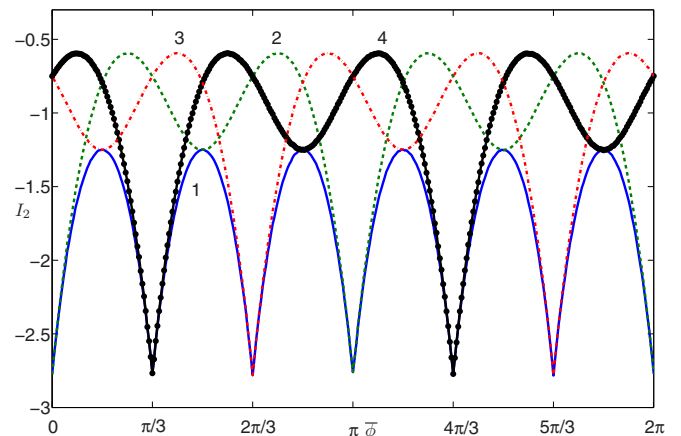


FIG. 4. (Color online) Plot showing the harmonic free energy contribution  $I_2$  for each of the four branches ( $A = 1, 2, 3, 4$ ) of ground states with the  $\bar{\phi}_a$  angle for each sublattice  $a = 2, 3, 4$  expressed in terms of  $\bar{\phi}_1$  via the parametrization given in Eq. (3). Each of the four curves is labeled by its ground state branch number taken from Eq. (3). Note, therefore, that the horizontal axis does not identify a unique spin configuration but rather a unique configuration for each of the four branches. The minima in the free energy appear where pairs of ground state branches meet—at the  $\psi_2$  spin configurations.

couple most strongly because fluctuations are responsible for effective fields perpendicular to the spin direction even in the broken-symmetry phase. The local  $XY$  and zero moment constraints of the  $XY$  pyrochlore antiferromagnet ensure that the spins cannot be collinear, but it is interesting to ask whether the  $\psi_2$  configurations are the most collinear states within the set of ground states. One finds that Eq. (10) is constant within the whole ground state manifold of Eq. (3). However, the sum  $-\sum_{i,j} |\mathbf{S}_i \cdot \mathbf{S}_j|$  is minimized by the  $\psi_2$  states which lends some credence to the intuition that the most collinear states among all the classically degenerate zero-temperature ground states must be selected.

### B. Quantum selection

Having shown semianalytically that thermal fluctuations select the  $\psi_2$  states, we now turn to the effect of quantum fluctuations which, in general, need not select the same states. In this section, we present the spin wave spectrum computed using the Holstein-Primakoff transformation treated in a large  $S$  expansion and truncated at harmonic order. The calculation is performed for the Hamiltonian in Eq. (1) with  $\mathcal{D} = 0$ . In the coordinate system with  $z$  axes taken along the  $\langle 111 \rangle$  directions, the Hamiltonian is written  $H = \sum \mathcal{J}_{ij}^{\alpha\beta} S_i^\alpha S_j^\beta$ , where  $\alpha$  and  $\beta$  denote the spin components. The local Ising components of the matrix of interactions  $\mathcal{J}_{ij}^{\alpha\beta}$  are set equal to zero—this imposes a soft  $XY$  constraint because the computation of the spin wave spectrum implicitly allows fluctuations out of the easy planes. This is somewhat relevant to the  $\text{Er}_2\text{Ti}_2\text{O}_7$  pyrochlore antiferromagnet whose single-ion crystal field doublet, characterized by an anisotropic  $g$  tensor with two eigenvalues such that  $g_\perp > g_\parallel$ , allows for a description in terms of an effective spin-1/2 model [38]. Working in reciprocal space with  $N$  spins and  $N_P$  primitive lattice sites, one rewrites the spin Hamiltonian in terms of boson operators, with [28,29]

$$\tilde{S}_a^z(\mathbf{k}) = \sqrt{N_P} S \delta_{\mathbf{k},0} e^{-i\mathbf{k}\cdot\mathbf{r}_a} - \frac{1}{\sqrt{N_P}} a_a^\dagger(\mathbf{k}') a_a(\mathbf{k}' - \mathbf{k}), \quad (11)$$

$$\tilde{S}_a^x(\mathbf{k}) = \sqrt{\frac{S}{2}} [a_a^\dagger(\mathbf{k}) + a_a(-\mathbf{k})], \quad (12)$$

$$\tilde{S}_a^y(\mathbf{k}) = i\sqrt{\frac{S}{2}} [a_a^\dagger(\mathbf{k}) - a_a(-\mathbf{k})], \quad (13)$$

on each site with the new  $z$  axis now taken to be the quantization axis. The quantization axis,  $z$ , is taken within the ground state manifold of the model with antiferromagnetic exchange as parametrized by local angles  $\bar{\phi}_a$  for  $a = 1, 2, 3, 4$  given in Eq. (3). There are four flavors of bosons corresponding to the distinct sublattices labeled with subscript  $a$ . One performs a Bogoliubov transformation taking boson operators  $a_a^\dagger(\mathbf{k})$  and  $a_a(\mathbf{k})$  into spin wave creation and annihilation operators  $c_A^\dagger(\mathbf{k})$  and  $c_A(\mathbf{k})$  so that the Hamiltonian to harmonic order is brought to the form

$$H[\bar{\phi}] = -NJS(S+1) + JS \sum_{\mathbf{k},A} \epsilon_A(\mathbf{k}) + JS \sum_{\mathbf{k},A} \epsilon_A(\mathbf{k}) c_A^\dagger(\mathbf{k}) c_A(\mathbf{k}), \quad (14)$$

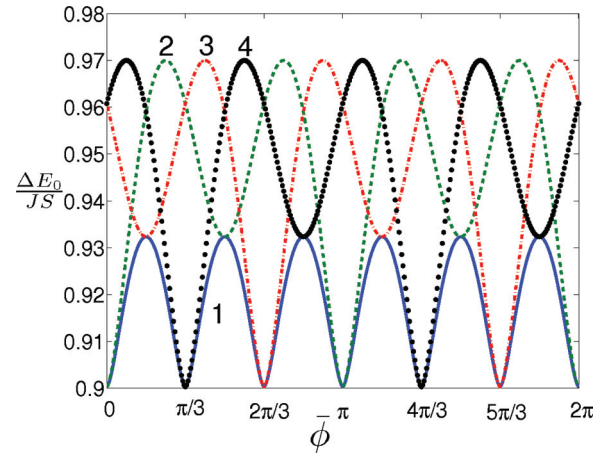


FIG. 5. (Color online) Zero point energy for the pyrochlore  $XY$  model from the linear spin wave spectrum computed from the classical ground states. The horizontal axis is the  $\phi$  parameter given in Eq. (3) and each curve carries a label identifying the branch of ground states to which it belongs. The quantum correction to the classical ground state energy is minimized for the  $\psi_2$  states.

where  $\epsilon_A(\mathbf{k})$  are the spin wave energies. Further details of Holstein-Primakoff linear spin waves on a pyrochlore lattice of spins can be found in Ref. [28]. As one would expect for an antiferromagnet, the dispersion for the model Eq. (1) about the zero modes is linear in  $|\mathbf{k}|$ . Just as in the classical case, the zero modes appear in pairs of planes in the first Brillouin zone for the  $\psi_2$  states. The harmonic correction to the ground state energy is

$$N \Delta E_0[\bar{\phi}] \equiv \left( \frac{NJS}{4} \times \frac{1}{4} \right) \sum_A \int_{\text{BZ}} \frac{d^3\mathbf{k}}{(2\pi)^3} \epsilon_A(\mathbf{k}), \quad (15)$$

which we have evaluated numerically. The results are shown in Fig. 5. To harmonic order, one observes that, among the  $\mathbf{q} = 0$  ground states, the zero-point energy is minimized at the  $\psi_2$  spin configurations ( $\bar{\phi}_a = n\pi/3$  for all  $a$ ), so a quantum order-by-disorder mechanism selects the same states as thermal fluctuations, as was originally speculated in Ref. [15].

### C. Monte Carlo results

To further confirm the thermal order-by-disorder mechanism argued for in Sec. IV A along with the concern, expressed in Ref. [16], that the  $\psi_2$  long-range order might not survive in the thermodynamic limit, we performed Monte Carlo simulations of the nearest-neighbor exchange only model. Parallel tempering Monte Carlo simulations were carried out with  $J = 1$  (and  $\mathcal{D} = 0$ ) for four different system sizes,  $L = 2, 3, 4$ , and 5, of  $L^3$  cubic unit cells of 16 spins. To equilibrate the system,  $5 \times 10^6$  Monte Carlo sweeps were performed, followed by the same number of steps to collect data. All four system sizes were found to have equilibrated satisfactorily according to the criteria discussed in Sec. III. We note that we were unable to obtain well-equilibrated results for  $L = 6$  even using parallel tempering. Equilibration close to the first-order transition for larger system sizes to the extent necessary to obtain satisfactory finite-size scaling would most likely require a new technique to explore the statistics

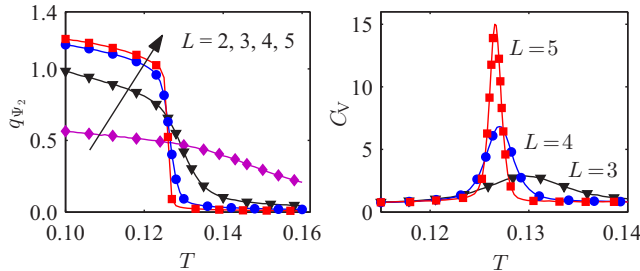


FIG. 6. (Color online) Order parameter  $q_{\psi_2}$  and heat capacity  $C_V$  as a function of temperature for  $J = 1$  and  $\mathcal{D} = 0$ . Left and right panels display results for  $q_{\psi_2}$  ( $L = 2, 3, 4, 5$ ) and for  $C_V$  ( $L = 3, 4, 5$ ), respectively.

of configurations with interfaces such as the multicanonical method [39,40], as employed in a model of dipolar spin ice [4], for example.

Figures 6, 7, and 8 show data from the Monte Carlo simulations for  $\mathcal{D}/J = 0$ . The left-hand panel of Fig. 6 shows the onset of the  $\psi_2$  order parameter while the right panel shows the temperature dependence of the specific heat,  $C_V$ , near  $T/J = 0.127$ , the estimated transition temperature, for various system sizes. We have found that this estimated transition temperature  $T_c/J \approx 0.127$  is consistent both with the one estimated from our sublattice magnetization results (not shown) and those of Ref. [16].

Both the rate of increase of the heat capacity peak and the jump in  $q_{\psi_2}$  with increasing  $L$  are consistent with a first-order phase transition in the thermodynamic limit. The left-hand panel of Fig. 7 is a histogram of the measured energies close to the transition temperature for  $L = 4$ . Its double-peaked structure is a clear indication of coexistence and hence of the first-order nature of the transition. The right panel of Fig. 7 shows how the peak height of the specific heat,  $C_{V,\max}$ , depends on the cube of the system size,  $L^3$ . For a first-order transition, one expects  $C_{V,\max} \propto (a + bL^3)$  in the limit of large  $L$  [41]. The plot illustrates that for  $L = 4$  ( $L^3 = 64$ ) and  $L = 5$  ( $L^3 = 125$ ),  $C_{V,\max}$  is approaching this expected behavior. This provides further evidence for a first-order transition in

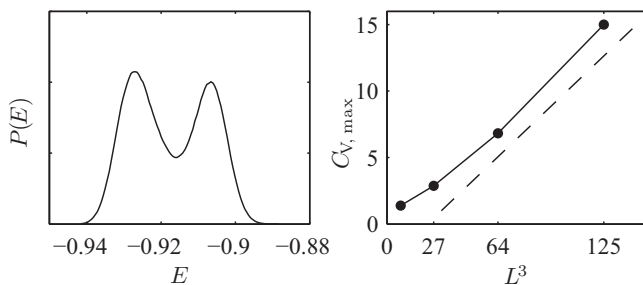


FIG. 7. Two plots showing Monte Carlo data for  $J = 1$  and  $\mathcal{D} = 0$  illustrating the first-order nature of the transition. The left-hand panel is a histogram of the measured energies for  $L = 4$  at  $T/J \approx 0.127$ , close to the transition temperature. The double-peaked structure is evidence for a coexistence region and hence an underlying first-order transition. The right panel shows the peak height of the specific heat,  $C_{V,\max}$ , versus the cube of the system size,  $L^3$ . The dashed line shows a straight line for the hypothetical  $C_{V,\max} \propto a + bL^3$  in the thermodynamic limit.

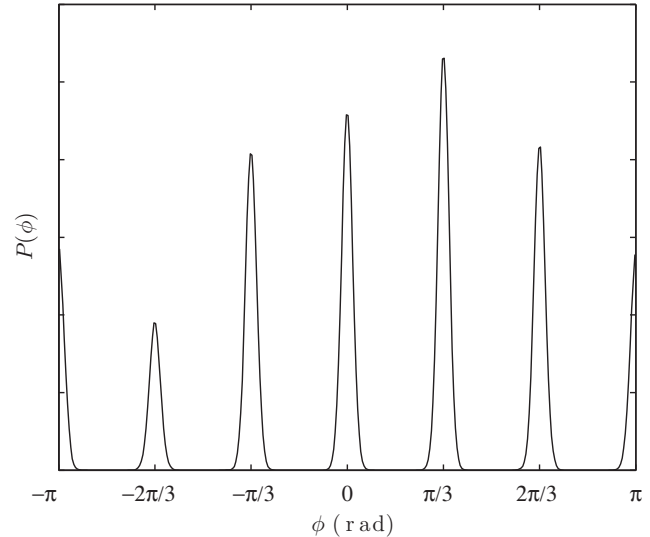


FIG. 8. Monte Carlo data for  $J = 1$  and  $\mathcal{D} = 0$ . Histogram of the local XY angles for all spins for  $L = 4$  at a temperature  $T/J = 0.1 \lesssim T_c$ . The histogram shows peaks at angles  $n\pi/3$  illustrating that the  $\psi_2$  states are preferably sampled below  $T_c/J \approx 0.127$ .

this  $\mathcal{D} = 0$  (111) pyrochlore XY antiferromagnet. Finally, Fig. 8 shows a histogram of the local XY angle averaged over all spins on all sublattices at  $T/J = 0.1$  for system size  $L = 4$ . The figure shows six sharp peaks concentrated at the  $\psi_2$  angles  $n\pi/3$ . We find, in addition, that the spin angles on all sublattices are concentrated around one of these angles at any given Monte Carlo time. This result therefore demonstrates the selection of  $\psi_2$  states from the continuous manifold of classical ground states and also that all six magnetic domains are sampled in the course of the simulation—a possibility facilitated by the use of a parallel tempering algorithm in our simulations compared to those of Refs. [14–16].

## V. PERTURBING THE XY PYROCHLORE ANTIFERROMAGNET

### A. Materials context

Recent years have seen a great deal of progress in the understanding of the rare-earth pyrochlore magnets [18]. Early successes came from studying the spin ices where geometrical frustration leads to an exotic state of matter which can be understood quantitatively on the basis of an Ising model with long-range interactions. Most of the available materials exist away from the Ising limit though. Here, progress has been possible by recognizing that the largest couplings in these magnets should, in general, have significant values of all four independent nearest-neighbor interactions allowed by symmetry [22–24,42,43]. For example, a set of anisotropic exchange couplings found for  $\text{Yb}_2\text{Ti}_2\text{O}_7$  by fitting spin wave data taken in a field-induced ordered state [42] has been shown to produce excellent agreement with heat capacity and field-dependent magnetization [44,45].

From this point of view, there is a danger that the XY pyrochlore antiferromagnet, as only one point in this high-dimensional space, might appear phenomenologically irrelevant. In reality, it turns out to influence the physics

over a broad range of couplings. The material  $\text{Er}_2\text{Ti}_2\text{O}_7$  undergoes a phase transition at a temperature  $T_c \sim 1.2$  K from a paramagnet to a long-range-ordered magnetic state with the  $\psi_2$  structure. Although the couplings in this material are highly anisotropic [46,47], it is not a coincidence that the  $XY$  antiferromagnet shares its ordered structure with  $\text{Er}_2\text{Ti}_2\text{O}_7$ . In this paper, we have reviewed the ground states of the  $XY$  antiferromagnet showing that there are four families of solutions each with a continuous degeneracy. The states selected by fluctuations lie at the intersections between these different families. When perturbations are added to the Hamiltonian, the branch labeled 1 in Sec. II remains degenerate as shown for nearest-neighbor couplings in Ref. [23] (and generalized to further neighbor couplings in Ref. [46]) *but, in general, the degeneracy of the remaining branches is lifted*. Even so, branch 1 remains the classical ground state for a wide range of couplings and the spin states at intersection points between branches,  $\psi_2$ , have softer modes than other spin configurations leading to order-by-disorder. This is the case for  $\text{Er}_2\text{Ti}_2\text{O}_7$ .

The softness of the modes at the  $\psi_2$  configurations can potentially lead to an interesting scenario where the classical ground state is not  $U(1)$  degenerate—the  $U(1)$  degenerate space of states whose energy is being *pushed above* some other states—but where thermal or quantum fluctuations *nevertheless* select the  $\psi_2$  states over the ground states of the model considered without fluctuations. Motivated by the fact that many rare-earth pyrochlores possess large magnetic moments, we consider the role of the long-range dipolar interaction as a natural perturbation to the  $XY$  antiferromagnet. Since branch 1 remains degenerate [46] even under this long-range interaction, there is a possibility that order-by-disorder operates for fairly large values of the magnetic moments compared to the exchange couplings. This fluctuation stabilization would be further enhanced were the interactions between the spins to include anisotropic nearest-neighbor pseudo-dipolar exchange [23,24] decreasing the energetic long-range dipolar stabilization of the Palmer-Chalker states [25] [see Eq. (3)]. One may even ask whether such OBD may occur when the classical degeneracy is broken by the long-range interaction at zero temperature through anharmonic spin wave interactions or at finite temperature again through nonlinear effects. In this paper, we explore the latter phenomenon numerically to see whether it operates near the critical temperature to the paramagnetic phase.

### B. Effect of competing nearest-neighbor pseudo-dipolar interaction

In this subsection, we look at the effect of introducing pseudo-dipolar interactions on the order-by-disorder in the  $\langle 111 \rangle$   $XY$  pyrochlore antiferromagnet. These couplings of dipolar form acting between nearest-neighbor moments may arise as a contribution to the superexchange in pyrochlore magnets [24]. We find that order-by-disorder into  $\psi_2$  states *survives* for sufficiently small pseudo-dipolar couplings and estimate the maximum value of the dipolar coupling strength  $D$  that permits  $\psi_2$  ordering.

A similar behavior is observed, albeit in a different context, in a model that tunes between the Heisenberg pyrochlore

antiferromagnet and the fcc Heisenberg antiferromagnet. In this model, thermal order-by-disorder, studied using Monte Carlo simulations, prevails over the energetically driven ordering identified within mean-field theory [48]. No transition was reported in Ref. [48] from the entropically selected ordered phase to the energetically ordered phase as the temperature of the system decreases. Another related example is the Heisenberg  $J_1$ - $J_2$  model on a pyrochlore lattice where the nearest-neighbor interaction is antiferromagnetic and the second-neighbor coupling ferromagnetic [49]. In this model, there is an intermediate temperature collinear phase which is selected by entropic fluctuations that gives way to a multi- $q$  structure at lower temperatures.

The dipolar interaction in the following is first taken to act solely between nearest neighbors. If for no other reason, such a model has the advantage of reducing the difficulty in equilibrating the system and hence decreases the computer simulation time. As stated above, effective spin-spin interactions of this type can arise in real pyrochlore magnets. From a more computational perspective, we also study this simplified model because (i) in combination with antiferromagnetic exchange, dipolar interactions between nearest neighbors select the same  $\psi_4$  magnetic order as the long-range dipolar interactions [25] and because (ii) we have found, through Monte Carlo simulations of a model with long-range dipolar interactions (see the following subsection V C), that the general conclusions of this subsection do not depend sensitively on retaining the full  $1/r^3$  long-range nature of the magnetostatic dipole-dipole interactions. All simulations were conducted using a parallel tempering algorithm.

Figures 9 and 10 show the heat capacities and order parameters  $q_{\psi_2}$  and  $q_{\psi_4}$  for different values of  $D/J$  (see Sec. III for a definition of  $q_{\psi_2}$  and  $q_{\psi_4}$ ). The first row of Fig. 9 shows the results for  $D/J = 0.5 \times 10^{-4}$  for  $L = 3, 4$ , and 5. There is a clear onset of the  $\psi_2$  order parameter upon lowering the temperature and this feature becomes *sharper* when the

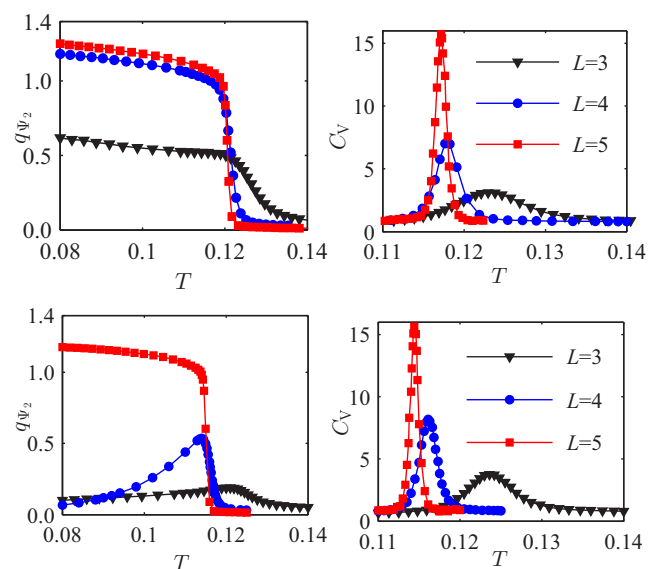


FIG. 9. (Color online) Order parameter  $q_{\psi_2}$  and heat capacity for  $L = 3, 4, 5$ , for  $D/J = 0.5 \times 10^{-4}$  and  $D/J = 10^{-4}$  in upper and lower panels, respectively.

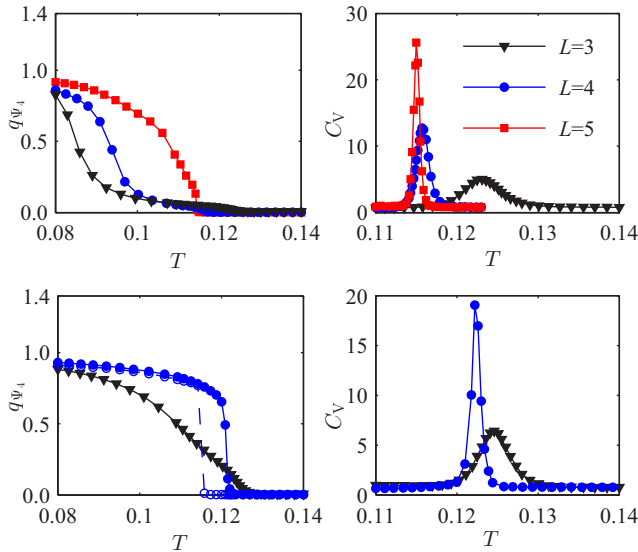


FIG. 10. (Color online) Order parameter  $q_{\psi_4}$  and heat capacity for  $\mathcal{D}/J = 2 \times 10^{-4}$  ( $L = 3, 4, 5$ ) and  $\mathcal{D}/J = 3 \times 10^{-4}$  ( $L = 3, 4$ ) in upper and lower panels, respectively. The dashed line shows unequilibrated data for  $L = 4$  when the simulation is started from a random initial configuration.

system size increases. Similar behavior is shown in the second row in Fig. 9 for a larger value,  $\mathcal{D}/J = 10^{-4}$ . The  $\psi_4$  order parameter was also measured for these two values of  $\mathcal{D}/J$  and found to be close to zero, within the present finite-size effects, and displaying no perceptible features around the onset temperature of  $q_{\psi_2}$ . This is, therefore, compelling evidence for the thermal order-by-disorder of an ordered  $\psi_2$  state at nonzero temperature that persist *despite* the presence of pseudo-dipolar interactions that energetically select a broken discrete symmetry ground state in such a way that the thermally selected states *are not* the true minimum energy classical states. Since the thermally selected states are not the true ground states, one expects a further phase transition at sufficiently low temperatures provided the system can be made to equilibrate. We have found no evidence for such a transition however using our parallel tempering algorithm.

In Fig. 10 all the simulations were started from the ordered  $q_{\psi_4}$  state. Due to the strongly first order character of the transition, it was not possible to equilibrate larger system sizes when starting from random initial conditions. For  $\mathcal{D}/J = 3 \times 10^{-4}$  we did not manage to equilibrate the  $L = 5$  system. The validity of the presented results were confirmed by comparison of the simulation started from both ordered and disordered initial configurations. In the case of  $L = 3$ , it was confirmed that simulations started from both ordered and disordered initial configurations give the same results. For larger  $L$ , it was observed that the simulation started from an ordered configuration essentially remains in this configuration, while the simulation started from a random initial condition slowly progresses toward the ordered state. The figure shows  $q_{\psi_4}$  for  $\mathcal{D}/J = 3 \times 10^{-4}$ , where the unequilibrated  $L = 4$  result for the simulation started from a random initial configuration is plotted with a dashed line.

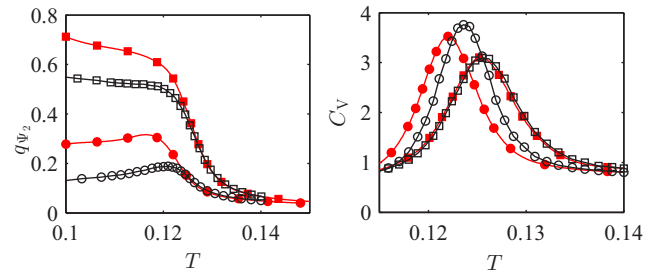


FIG. 11. (Color online) Order parameter  $q_{\psi_2}$  and heat capacity ( $L = 3$ ) for nearest-neighbor pseudo-dipolar interactions (solid red symbols) and long-range dipolar interactions (open black symbols). Squares mark the results for  $\mathcal{D}/J = 0.5 \times 10^{-4}$  and circles for  $\mathcal{D}/J = 10^{-4}$ .

### C. Effect of competing long-range dipolar interaction

In this subsection, we compare the data for the nearest-neighbor pseudo-dipolar interactions with the data obtained for long-range dipolar interaction treated with the Ewald method [50]. Including a full long-range dipolar interaction increases the scaling of the computational time from  $L^3$ , characterizing short-range models, to  $L^6$ . This, in combination with the very slow equilibration of the system, which was already encountered in the case of the nearest-neighbor pseudo-dipolar model, makes the simulation times for models with long-range interactions prohibitively long for all system sizes  $L > 3$ . To make further progress on this problem would necessitate the development of a more adequate simulation algorithm perhaps making better use of the aforementioned spatially extended excitations.

Figure 11 shows the order parameters  $q_{\psi_2}$  and heat capacities for  $L = 3$ , for two values of  $\mathcal{D}/J$ ,  $\mathcal{D}/J = 0.5 \times 10^{-4}$ , and  $\mathcal{D}/J = 10^{-4}$ , in the regime where the system orders into the  $\psi_2$  state at the critical temperature. The red solid symbols mark the data obtained with full Ewald treatment of the long-range dipolar interaction, while the black open symbols are the results for the nearest-neighbor pseudo-dipolar interactions repeated, for ease of comparison, from Fig. 9. There are only quantitative differences between the two data sets. In a similar fashion, Fig. 12 shows data for the regime where the system orders into the  $\psi_4$  state. The data obtained with Ewald method is marked with red solid symbols, while the data for

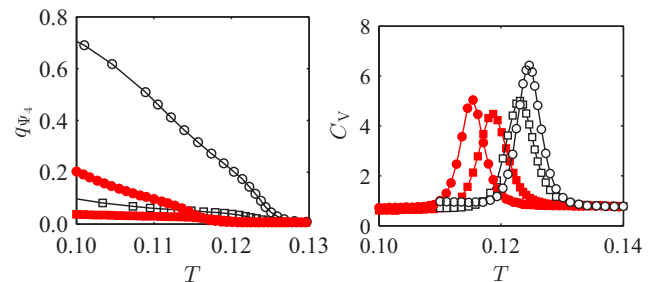


FIG. 12. (Color online) Order parameter  $q_{\psi_4}$  and heat capacity ( $L = 3$ ) for nearest-neighbor pseudo-dipolar interactions (solid red symbols) and long-range dipolar interactions (open black symbols). Squares mark the results for  $\mathcal{D}/J = 2 \times 10^{-4}$  and circles for  $\mathcal{D}/J = 3 \times 10^{-4}$ .

nearest-neighbor pseudo-dipolar interaction is indicated by black open symbols. The values of  $\mathcal{D}/J$  are  $\mathcal{D}/J = 2, 3 \times 10^{-4}$ . For both long- and short-ranged dipolar interactions the magnitude of the  $\psi_4$  order parameter increases with the relative strength of the dipolar interaction. The transition temperature in the case of the long-range dipolar interaction is higher than for the nearest-neighbor pseudo-dipolar interaction.

## VI. SUMMARY

We have discussed in Secs. II and IV, in some detail, the classical ground states, along with the thermal and quantum behavior of the pyrochlore  $\langle 111 \rangle$  XY antiferromagnet with exchange only.

We have shown that the classical ground states on a single tetrahedron have four branches of ground states each with one continuous degenerate set of states involving the smooth rotation of all four spins simultaneously, confirming the previous result [16]. From a calculation of the ground states on a single tetrahedron, we have inferred the ground states on the whole pyrochlore lattice which include line defects implying that the number of ground states scales as  $L^2$ , where  $L$  is the edge length of the crystal.

Monte Carlo simulations of this model confirm that there is thermal selection of a discrete set of spin states with ordering wave vector  $\mathbf{q} = 0$ , referred to as  $\psi_2$  states [19], from the manifold of classical ground states. We have shown, furthermore, that this selection occurs to harmonic order in small angular fluctuations about the classical ground states. In this model, the linear spin wave spectrum shows strong similarities with the spectrum of eigenvalues of the Hessian. Specifically, the spin wave zero modes and the Hessian zero modes appear within the same planes in reciprocal space for the  $\psi_2$  states. It follows that the quantum zero point energy is minimized at the same  $\psi_2$  spin configurations that are selected through a classical thermal order-by-disorder mechanism, hence confirming the conjecture of Refs. [15,16]. Knowledge of the classical ground states provides insight, from direct space rather than reciprocal space, into the nature of the fluctuation-induced long-range order that occurs in this model.

We have considered the effect of including (nearest-neighbor) pseudo-dipolar interactions together with the antiferromagnetic exchange in the classical model at finite temperature. The (energetically selected) ground states of this model are the  $\psi_4$  states [19] (also referred to as the Palmer-Chalker state [25]), given in Sec. II, so the introduction of dipolar interactions produces a competition between energetic selection and thermal selection. We have found evidence for the persistence of an order-by-disorder transition to a  $\psi_2$  state even when  $\mathcal{D} \neq 0$ . This finding implies that, in principle, a second transition should occur at lower temperatures into the  $\psi_4$  (Palmer-Chalker) long-range-ordered state since it is the nondegenerate and stable classical ground state. However, using Monte Carlo simulations, we have found no evidence for such a transition, at the very least, because the difficulties of equilibration within the ordered  $\psi_2$  phase prevent the exploration of the space of configurations computationally. As remarked on in the previous section, a similar situation arises in the model of Refs. [48,49].

To conclude, we have shown that  $\psi_2$  long-range order is present at low temperatures in the  $\langle 111 \rangle$  XY pyrochlore antiferromagnet induced both by thermal and quantum fluctuations and we have gained insight from both direct and reciprocal space into why the  $\psi_2$  states are selected. The physics of this model controls a significant portion of the phase diagram within the space of symmetry-allowed anisotropic nearest-neighbor interactions [20,22–24,46]. We have also studied a case where the classical ground state degeneracy is broken down to a discrete set of states but where order-by-disorder operates at finite temperature. We expect the order-by-disorder mechanism to be somewhat robust to the presence of symmetry-breaking perturbations so much so that, experimentally, the typical case of thermal order-by-disorder may be accompanied by a low-temperature metastability of the states selected by thermal fluctuations with, perhaps, a failure of the system to reach its true classical zero-temperature ground state.

This kind of physics is perhaps relevant to the puzzling behavior observed in  $\text{Er}_2\text{Sn}_2\text{O}_7$ , a material closely related to  $\text{Er}_2\text{Ti}_2\text{O}_7$ , which does not develop long-range order down to 100 mK, but instead exhibits a freezing below a temperature of 200 mK that coexists with short-range Palmer-Chalker-like correlations [51].

*Note added in proof.* A paper discussing the general topic of finite-temperature and quantum order-by-disorder in XY pyrochlore magnets has recently appeared [52]. Also, a recent paper reporting inelastic neutron scattering measurements on  $\text{Er}_2\text{Ti}_2\text{O}_7$  [53] finds evidence for a zone center spin-wave gap of approximately 0.05 meV, as is necessary for a broken discrete symmetry  $\psi_2$  long-range ordered state [21,46], as opposed to a gapless Goldstone mode [15]. (See Refs. [54,55] for previous reports on an upper bound on the value of this gap).

## ACKNOWLEDGMENTS

We thank Bruce Gaulin, Peter Holdsworth, Kate Ross, Jacob Ruff and Jordan Thompson for useful discussions. This research was supported by the NSERC of Canada, the Canada Research Chair program (M.G., Tier I), and the Perimeter Institute for Theoretical Physics. Research at PI is supported by the Government of Canada through Industry Canada and by the Province of Ontario through the Ministry of Economic Development and Innovation. We acknowledge the use of the computing facilities of the Shared Hierarchical Academic Research Computing Network (SHARCNET; <http://www.sharcnet.ca>).

## APPENDIX A: CALCULATION OF THE GROUND STATES OF THE XY ANTIFERROMAGNET

The zero-moment conditions on a single tetrahedron are

$$\cos(\phi_1) + \cos(\phi_2) = \cos(\phi_3) + \cos(\phi_4), \quad (\text{A1})$$

$$\cos(\phi'_1) + \cos(\phi'_4) = \cos(\phi'_2) + \cos(\phi'_3), \quad (\text{A2})$$

$$\cos(\phi''_1) + \cos(\phi''_3) = \cos(\phi''_2) + \cos(\phi''_4), \quad (\text{A3})$$

where  $\phi'_a \equiv \phi_a + \frac{2\pi}{3}$  and  $\phi''_a \equiv \phi_a + \frac{4\pi}{3}$ . The angles  $\phi_a$  are angles in the local coordinate system on sublattice  $a$  ( $a = 1, 2, 3, 4$ ). As discussed in Sec. II, and as previously

reported in Ref. [17], the ground states of the  $\langle 111 \rangle$  XY pyrochlore antiferromagnet are characterized by the following four sets of solutions (“branches”):

$$\begin{aligned} \text{branch 1: } & \bar{\phi} \equiv \bar{\phi}_1 = \bar{\phi}_2 = \bar{\phi}_3 = \phi_4, \\ \text{branch 2: } & \bar{\phi} \equiv \bar{\phi}_1 = \bar{\phi}_2 = -\bar{\phi}_3 = -\bar{\phi}_4, \\ \text{branch 3: } & \bar{\phi} \equiv \bar{\phi}_1 = \bar{\phi}_3, \quad \frac{4\pi}{3} - \bar{\phi} = \bar{\phi}_2 = \bar{\phi}_4, \\ \text{branch 4: } & \bar{\phi} \equiv \bar{\phi}_1 = \bar{\phi}_4, \quad \frac{2\pi}{3} - \bar{\phi} = \bar{\phi}_2 = \bar{\phi}_3. \end{aligned} \quad (\text{A4})$$

In this appendix, we present a derivation of this result that differs from the one in Ref. [17]. Defining  $\sigma_{ab} \equiv (\phi_a + \phi_b)/2$  and  $\delta_{ab} \equiv (\phi_a - \phi_b)/2$ , we first proceed to rewrite the zero-moment conditions as

$$\cos(\sigma_{12}) \cos(\delta_{12}) - \cos(\sigma_{34}) \cos(\delta_{34}) = 0, \quad (\text{A5})$$

$$-\sin(\sigma_{12}) \sin(\delta_{12}) + \sqrt{3} \cos(\sigma_{34}) \cos(\delta_{34}) = 0, \quad (\text{A6})$$

$$\sqrt{3} \cos(\sigma_{12}) \sin(\delta_{12}) - \sin(\sigma_{34}) \sin(\delta_{34}) = 0, \quad (\text{A7})$$

by using half-angle formulas and then combining the second and third zero-moment conditions in Eq. (A3) to finally obtain Eqs. (A6) and (A7).

Our strategy is to eliminate the sums of pairs,  $\sigma_{\mu\nu}$ , keeping only the differences of pairs,  $\delta_{\mu\nu}$ . Thus, from Eq. (A5), we get

$$\sin^2(\sigma_{12}) = 1 - \left( \frac{\cos(\sigma_{34}) \cos(\delta_{34})}{\cos(\delta_{12})} \right)^2.$$

Substitute into Eq. (A6) to get

$$\begin{aligned} [1 - \sin^2(\delta_{12}) - \cos^2(\delta_{34}) \cos^2(\sigma_{34})] \sin^2(\delta_{12}) \\ = 3 \cos^2(\sigma_{34}) \sin^2(\delta_{34}) [1 - \sin^2(\delta_{12})]. \end{aligned} \quad (\text{A8})$$

Then, squaring Eqs. (A6) and (A7), and adding the result, we obtain

$$\sin^2(\delta_{12}) = \left( \frac{1}{3} \sin^2(\sigma_{34}) + 3 \cos^2(\sigma_{34}) \right) \sin^2(\delta_{34}), \quad (\text{A9})$$

which we can otherwise write as

$$\cos^2(\sigma_{34}) = \frac{3}{8} \left( \frac{\sin^2(\delta_{12})}{\sin^2(\delta_{34})} - \frac{1}{3} \right). \quad (\text{A10})$$

So now we can proceed with what we set out to do: substitute Eq. (A10) into Eq. (A8) leaving us, after rearranging and canceling off a  $\cos^2(\delta_{12})$  term, with

$$\begin{aligned} \sin^2(\delta_{12}) \sin^2(\delta_{34}) = \frac{1}{8} [3 \sin^2(\delta_{12}) - \sin^2(\delta_{34})] \\ \times [3 \sin^2(\delta_{34}) + \sin^2(\delta_{12})]. \end{aligned} \quad (\text{A11})$$

It follows from this last equation that

$$\frac{3}{8} [\sin^2(\delta_{34}) - \sin^2(\delta_{12})] = 0.$$

Hence, the most general form for the set of  $\phi_a$  angles is

$$(\bar{\phi}_1, \bar{\phi}_2, \bar{\phi}_3, \bar{\phi}_4) = (\bar{\phi} + \theta, \bar{\phi}, \psi \pm \theta, \psi).$$

Substituting this into our original zero moment formula, Eq. (A1), which we write here again,

$$\cos(\bar{\phi}_1) + \cos(\bar{\phi}_2) = \cos(\bar{\phi}_3) + \cos(\bar{\phi}_4),$$

shows that one must have either

$$(\bar{\phi}_1, \bar{\phi}_2, \bar{\phi}_3, \bar{\phi}_4) = (\phi + \theta, \phi, \phi + \theta, \phi)$$

or

$$(\bar{\phi}_1, \bar{\phi}_2, \bar{\phi}_3, \bar{\phi}_4) = (\phi + \theta, \phi, \phi, \phi + \theta)$$

if  $\theta$  is nonvanishing or

$$(\bar{\phi}_1, \bar{\phi}_2, \bar{\phi}_3, \bar{\phi}_4) = (\phi, \phi, \pm \phi, \pm \phi)$$

if  $\theta = 0$ . Thus, the angles must occur in pairs. One can now return to original zero-moment conditions, Eq. (A3), and, with the knowledge that the angles must occur in pairs, obtain the four branches of ground states in Eq. (A4). For example, suppose that the pairs of angles occur in the configuration

$$(\psi, \phi, \phi, \psi);$$

then Eq. (A3) gives the branch

$$\left( \psi, \frac{2\pi}{3} - \psi, \frac{2\pi}{3} - \psi, \psi \right),$$

which is the branch number 4 of Eq. (A4).

## APPENDIX B: BRILLOUIN ZONE INTEGRATION

In the calculation of the free energy in Eq. (9), in particular the last term of that equation, we take the Brillouin zone sum over to an integral as applicable to the case of an infinite lattice. In general, we expect

$$\sum_{\mathbf{k}} \rightarrow \frac{N_P}{\Omega_{\text{BZ}}} \int_{\text{BZ}},$$

where the integral is taken over the Brillouin zone of volume  $\Omega_{\text{BZ}}$  and  $N_P$  is the number of primitive cells. We thus have

$$\sum_{\mathbf{k}} \rightarrow \frac{Na^3}{4[4(2\pi)^3]} \int_{\text{BZ}} d^3k.$$

The edge length of the cubic unit cell,  $a$ , has been set equal to 1. The two factors of one-quarter come about because (i)  $4N_P = N$  where  $N$  is the number of spins and (ii) the Brillouin zone volume is  $4(2\pi/a)^3$ .

## APPENDIX C: EQUIPARTITION ARGUMENT

In this appendix, we revisit the Monte Carlo simulations presented in Ref. [16]. In particular, we consider Fig. 6 in that work showing the average energy in the ordered phase at low temperatures as a function of the system size. The authors of Ref. [16] found that

$$\frac{E}{Nk_B T} = \alpha - \beta \frac{1}{L}.$$

We find that the existence of chains of zero modes in the  $\langle 111 \rangle$  XY pyrochlore antiferromagnet is sufficient to constrain the coefficients  $\alpha$  and  $\beta$ .

Let us consider a cubic cell with edge length  $L$  with each cubic unit cell of unit edge length. The number of spins is  $N = 16L^3$ . Consider a square face of a single cubic cell. There are two chains beginning on the face that alternate between sublattices  $a$  and  $b$ . The number of such chains passing through the sample is  $N_{\text{chains}} = 2L^2$ . There is one degree of freedom per spin so the average energy would be  $(1/2)NkT$  were it not for the fact that the spectrum of modes about the  $\psi_2$  states has planes of zero modes. We shall assume that the zero modes (in the harmonic spectrum) are actually resolved by a quartic contribution to the energy, when looking at the higher order corrections to the Hamiltonian, giving a thermal energy of  $k_B T/4$  per quartic mode. The zero modes correspond to rotations along two classes of  $ab$  chains so the number of

such modes is  $2N_{\text{chains}}$ . Thus, the average energy is

$$\begin{aligned} E &= \frac{k_B T}{2}(N - 2N_{\text{chains}}) + \frac{k_B T}{4}(2N_{\text{chains}}) \\ &= \frac{k_B T}{2}N - \frac{k_B T}{2}N_{\text{chains}}. \end{aligned}$$

Then, because  $N_{\text{chains}} = 2L^2 = 2(N/16)^{2/3}$ , we obtain

$$\frac{E}{Nk_B T} = \frac{1}{2} - \frac{1}{16^{2/3}}N^{-1/3} = \frac{1}{2} - \frac{1}{16} \frac{1}{L}.$$

The coefficient in front of  $1/L$  from Monte Carlo simulation [16] is approximately 0.0636 which is in good agreement with the calculated  $1/16 = 0.06250$  value above.

- 
- [1] G. H. Wannier, *Phys. Rev.* **79**, 357 (1950); R. M. F. Houtappel, *Physica* **16**, 425 (1950).
- [2] S. T. Bramwell and M. J. P. Gingras, *Science* **294**, 1495 (2001).
- [3] M. J. P. Gingras and B. C. den Hertog, *Can. J. Phys.* **79**, 1339 (2001).
- [4] R. G. Melko and M. J. P. Gingras, *J. Phys.: Condens. Matter* **16**, R1277 (2004); R. G. Melko, B. C. den Hertog, and M. J. P. Gingras, *Phys. Rev. Lett.* **87**, 067203 (2001).
- [5] S. V. Isakov, R. Moessner, and S. L. Sondhi, *Phys. Rev. Lett.* **95**, 217201 (2005).
- [6] B. C. den Hertog and M. J. P. Gingras, *Phys. Rev. Lett.* **84**, 3430 (2000).
- [7] H. Fukazawa, R. G. Melko, R. Higashinaka, Y. Maeno, and M. J. P. Gingras, *Phys. Rev. B* **65**, 054410 (2002); K. Matsuhira, Y. Hinatsu, K. Tenya, and T. Sakakibara, *J. Phys. Condens. Matter* **12**, L649 (2000); J. Snyder, J. S. Slusky, R. J. Cava, and P. Schiffer, *Nature (London)* **413**, 48 (2001).
- [8] D. Pomaranski, L. R. Yaraskavitch, S. Meng, K. A. Ross, H. M. L. Noad, H. A. Dabkowska, B. D. Gaulin, and J. B. Kycia, *Nat. Phys.* **9**, 353 (2013).
- [9] J. Villain, *Z. Physik B* **33**, 31 (1979).
- [10] C. L. Henley, *Phys. Rev. Lett.* **62**, 2056 (1989).
- [11] E. F. Shender, *Zh. Eksp. Theor. Fiz.* **83**, 326 (1982) [*Sov. Phys. JETP* **56**, 178 (1982)]; T. Yildirim, A. B. Harris, and E. F. Shender, *Phys. Rev. B* **53**, 6455 (1996); T. Yildirim, *Turk. J. Phys.* **23**, 47 (1999).
- [12] Refs. [9–11] discuss a small assortment of models that exhibit order-by-disorder of some variety.
- [13] R. Moessner and J. T. Chalker, *Phys. Rev. Lett.* **80**, 2929 (1998); *Phys. Rev. B* **58**, 12049 (1998).
- [14] S. T. Bramwell, M. J. P. Gingras, and J. N. Reimers, *J. Appl. Phys.* **75**, 5523 (1994).
- [15] J. D. M. Champion, M. J. Harris, P. C. W. Holdsworth, A. S. Wills, G. Balakrishnan, S. T. Bramwell, E. Čížmár, T. Fennell, J. S. Gardner, J. Lago, D. F. McMorro, M. Orendáč, A. Orendáčová, D. McK. Paul, R. I. Smith, M. T. F. Telling, and A. Wildes, *Phys. Rev. B* **68**, 020401(R) (2003).
- [16] J. D. M. Champion and P. C. W. Holdsworth, *J. Phys. Condens. Matter* **16**, S665 (2004).
- [17] J. D. M. Champion, Ph.D. thesis, University of London, 2001.
- [18] J. S. Gardner, M. J. P. Gingras, and J. E. Greedan, *Rev. Mod. Phys.* **82**, 53 (2010).
- [19] A. Poole, A. S. Wills, and E. Lelièvre-Berna, *J. Phys. Condens. Matter* **19**, 452201 (2007).
- [20] M. E. Zhitomirsky, M. V. Gvozdikova, P. C. W. Holdsworth, and R. Moessner, *Phys. Rev. Lett.* **109**, 077204 (2012).
- [21] P. Stasiak, P. A. McClarty, and M. J. P. Gingras, *arXiv:1108.6053*.
- [22] S. H. Curnoe, *Phys. Rev. B* **78**, 094418 (2008).
- [23] P. A. McClarty, S. H. Curnoe, and M. J. P. Gingras, *J. Phys.: Conf. Ser.* **145**, 012032 (2009).
- [24] J. D. Thompson, P. A. McClarty, H. M. Rønnow, L. P. Regnault, A. Sørge, and M. J. P. Gingras, *Phys. Rev. Lett.* **106**, 187202 (2011).
- [25] S. E. Palmer and J. T. Chalker, *Phys. Rev. B* **62**, 488 (2000).
- [26] In  $\text{Er}_2\text{Ti}_2\text{O}_7$ , the moments have a significant  $XY$  single-ion anisotropy which is reflected in  $g_{\perp} > g_{\parallel}$ . See Refs. [15, 46].
- [27] We point out that the Palmer-Chalker states [25] which we refer to as  $\psi_4$  states are denoted  $\psi_3$  in Ref. [15]. We abide by the notation of Ref. [19].
- [28] A. G. Del Maestro and M. J. P. Gingras, *J. Phys.: Condens. Matter* **16**, 3339 (2004).
- [29] A. G. Del Maestro and M. J. P. Gingras, *Phys. Rev. B* **76**, 064418 (2007).
- [30] A. S. Wills, M. E. Zhitomirsky, B. Canals, J. P. Sanchez, P. Bonville, P. Dalmas de Reotier, and A. Yaouanc, *J. Phys.: Condens. Matter* **18**, L37 (2006); J. R. Stewart, J. S. Gardner, Y. Qiu, and G. Ehlers, *Phys. Rev. B* **78**, 132410 (2008).
- [31] J. A. Quilliam, K. A. Ross, A. G. Del Maestro, M. J. P. Gingras, L. R. Corruccini, and J. B. Kycia, *Phys. Rev. Lett.* **99**, 097201 (2007).
- [32] J. R. Stewart, G. Ehlers, A. S. Wills, S. T. Bramwell, and J. S. Gardner, *J. Phys.: Condens. Matter* **16**, 321 (2004); J. S. Gardner, J. R. Stewart, and G. Ehlers, *AIP Conf. Proc.* **1202**, 3 (2010).
- [33] B. Javanparast, Z. Hao, M. Enjalran, and M. J. P. Gingras, *arXiv:1310.5146*.
- [34] E. Marinari and G. Parisi, *Europhys. Lett.* **19**, 451 (1992); K. Hukushima and K. Nemoto, *J. Phys. Soc. Jpn.* **65**, 1604 (1996).
- [35] M. Enjalran and M. J. P. Gingras, *Phys. Rev. B* **70**, 174426 (2004).

- [36] O. Cépas, A. P. Young, and B. S. Shastry, *Phys. Rev. B* **72**, 184408 (2005).
- [37] The free energy is a smooth function of the parameter that tunes between classical ground states despite the presence of zeros in the eigenvalues of the Hessian. This is because the zeros occur on planes in the Brillouin zone. Consider a plane of zeros in the  $yz$  plane with linear dispersion (for an antiferromagnet) giving a  $k_x$  dispersion for small  $k_x$  away from the plane of zeros. The free energy is, roughly, the integral over the Brillouin zone of  $\ln k_x$  or
- $$\int_0^{k_0} dk_x \ln |k_x|,$$
- where the upper (positive) limit is arbitrary. This integral is finite.
- [38] See the Supplemental Material of Ref. [24] for a related discussion for the XY pyrochlore ferromagnet  $\text{Yb}_2\text{Ti}_2\text{O}_7$ .
- [39] B. A. Berg and T. Neuhaus, *Phys. Rev. Lett.* **68**, 9 (1992).
- [40] U. H. E. Hansmann and Y. Okamoto, *Physica A* **212**, 415 (1994).
- [41] K. Binder and D. W. Heermann, *Monte Carlo Simulation in Statistical Physics, 3rd ed.* (Springer, Berlin, 1997).
- [42] K. A. Ross, L. Savary, B. D. Gaulin, and L. Balents, *Phys. Rev. X* **1**, 021002 (2011).
- [43] H. Cao, A. Gukasov, I. Mirebeau, P. Bonville, C. Decorse, and G. Dhalenne, *Phys. Rev. Lett.* **103**, 056402 (2009).
- [44] R. Applegate, N. R. Hayre, R. R. P. Singh, T. Lin, A. G. R. Day, and M. J. P. Gingras, *Phys. Rev. Lett.* **109**, 097205 (2012).
- [45] N. R. Hayre, K. A. Ross, R. Applegate, T. Lin, R. R. P. Singh, B. D. Gaulin, and M. J. P. Gingras, *Phys. Rev. B* **87**, 184423 (2013).
- [46] L. Savary, K. A. Ross, B. D. Gaulin, J. P. C. Ruff, and L. Balents, *Phys. Rev. Lett.* **109**, 167201 (2012).
- [47] J. Oitmaa, R. R. P. Singh, B. Javanparast, A. G. R. Day, B. V. Bagheri, and M. J. P. Gingras, *Phys. Rev. B* **88**, 220404(R) (2013).
- [48] C. Pinettes, B. Canals, and C. Lacroix, *Phys. Rev. B* **66**, 024422 (2002).
- [49] D. Tsuneishi, M. Ioki, and H. Kawamura, *J. Phys.: Condens. Matter* **19**, 145273 (2007); G.-W. Chern, R. Moessner, and O. Tchernyshyov, *Phys. Rev. B* **78**, 144418 (2008); T. Okubo, T. H. Nguyen, and H. Kawamura, *ibid.* **84**, 144432 (2011).
- [50] P. Ewald, *Ann. Phys.* **369**, 253 (1921); S. W. De Leeuw, J. W. Perram, and E. R. Smith, *Proc. R. Soc. London, Ser. A* **373**, 27 (1980); Z. Wang and C. Holm, *J. Chem. Phys.* **115**, 6351 (2001).
- [51] S. Guitteny, S. Petit, E. Lhotel, J. Robert, P. Bonville, A. Forget, and I. Mirebeau, *Phys. Rev. B* **88**, 134408 (2013).
- [52] H. Yan, O. Benton, L. D. C. Jaubert, and N. Shannon, [arXiv:1311.3501](https://arxiv.org/abs/1311.3501).
- [53] K. A. Ross, Y. Qiu, J. R. D. Copley, H. A. Dabkowska, and B. D. Gaulin, [arXiv:1401.1176](https://arxiv.org/abs/1401.1176) [Phys. Rev. Lett. (to be published)].
- [54] S. S. Sosin, L. A. Prozorova, M. R. Lees, G. Balakrishnan, and O. A. Petrenko, *Phys. Rev. B* **82**, 094428 (2010).
- [55] P. Dalmas de Réotier, A. Yaouanc, Y. Chapuis, S. H. Curnoe, B. Grenier, E. Ressouche, C. Marin, J. Lago, C. Baines, and S. R. Giblin, *Phys. Rev. B* **86**, 104424 (2012).